

A Novel Flavonoid Derivative of Icariside II (YS-10) Improves Erectile Dysfunction in a Diabetic Rat Model by Inhibiting Ferroptosis via Activation of the Nrf2/HO-1/GPX4 Pathway

Yang Liu^{1,2}, Guan-nan Liu^{1,2}, Ya-rong Zha¹, Chen-li Pan¹, Yong-de Xu³, Hong-wei Li¹, Yue-yue Zang¹, Wan-qi Wang¹, Jun-jie Yao¹, Jun-tao Sun^{1,2}, Yong Yang², Zhi-tao Wei²

¹Changchun University of Chinese Medicine, Changchun, Jilin Province, People's Republic of China; ²Department of Urology, The Affiliated Hospital of Changchun University of Chinese Medicine, Changchun, Jilin Province, People's Republic of China; ³Department of Urology, Beijing Friendship Hospital, Capital Medical University, Beijing, 100050, People's Republic of China

Correspondence: Yong Yang; Zhi-tao Wei, Department of Urology, The Affiliated Hospital of Changchun University of Chinese Medicine, Changchun, Jilin Province, 130021, People's Republic of China, Email yangyong@ccucm.edu.cn; dr_sirius@163.com

Objective: This study aimed to evaluate the therapeutic potential of YS-10, a novel flavonoid derivative of icaricidin II (ICA II), and to explore its mechanism of action in a diabetic rat model of erectile dysfunction (DMED).

Methods: Twenty-four male Sprague-Dawley rats were divided into four groups: control, DMED, DMED + ICA II (2.5 mg/kg/day), and DMED + YS-10 (2.5 mg/kg/day). Treatments lasted for 4 weeks followed by a 3-day washout. Erectile function was assessed, and penile tissues were analyzed by histology, immunohistochemistry, ELISA, and Western blot. In vitro, primary corpus cavernosum endothelial cells (CCECs) were treated with advanced glycation end products (AGEs), YS-10, Fer-1 (ferroptosis inhibitor), or ML385 (Nrf2 inhibitor) to evaluate oxidative stress and ferroptosis.

Results: In vivo, both YS-10 and ICA II (2.5 mg/kg/day) significantly improved erectile function in diabetic rats, increased smooth muscle content, reduced collagen deposition, and enhanced endothelial marker (CD31) expression in penile tissue ($p < 0.01$ vs DMED group). The maximum ICP/MAP ratio and oxidative stress markers were similarly restored in both treatment groups, with no significant difference between YS-10 and ICA II ($p > 0.05$). In vitro, YS-10 reversed AGEs-induced injury and ferroptosis in corpus cavernosum endothelial cells (CCECs), upregulated GPX4, downregulated ACSL4, and reduced ROS and lipid peroxidation, comparable to the effects of the ferroptosis inhibitor Fer-1. YS-10 also promoted Nrf2 nuclear translocation and elevated HO-1 expression. Molecular docking, immunofluorescence, and Western blot confirmed the interaction between YS-10 and the Nrf2/HO-1/GPX4 signaling pathway.

Conclusion: YS-10 improves erectile function in diabetic rats by reducing oxidative stress and inhibiting ferroptosis via activation of the Nrf2/HO-1/GPX4 pathway. At 2.5 mg/kg/day, YS-10 was effective, well-tolerated, and showed efficacy comparable to ICA II. These findings support its potential as a promising candidate for diabetes-related erectile dysfunction therapy.

Keywords: diabetes mellitus, erectile dysfunction, ferroptosis, YS-10, ICA II, Nrf2, GPX4

Introduction

Erectile dysfunction (ED) is a widespread condition among adult men, with a notably higher prevalence in individuals with diabetes. Patients with diabetes mellitus erectile dysfunction (DMED) have an earlier age of onset, are more severely affected, and the incidence of the disease increases with the duration of the disease compared to non-diabetic ED patients. It has been shown that diabetic patients are 3.5 times more likely to develop ED than healthy men, with approximately 37.5% of type 1 diabetic patients suffering from ED.¹ The etiology of DMED is complex and varied, and mainly includes oxidative stress, vascular endothelial dysfunction, neuropathy,

and chronic hyperglycemia induced advanced glycation end products (AGEs), and other aspects.² For example, AGEs produced in a hyperglycemic environment reduce penile corpus cavernosum extensibility and alter nitric oxide (NO) levels and function, thereby affecting erections. These deleterious factors lead to oxidative stress.^{3,4} Oxidative stress is the production of reactive oxygen species (ROS) in the body that exceeds the scavenging capacity of antioxidant mechanisms, leading to cell and tissue damage. In diabetic patients, the production of ROS is significantly increased due to hyperglycemia and metabolic disorders, as oxidative stress in the cavernous tissues of the penis is closely related to the impairment of endothelial function, which ultimately leads to reduced blood flow and ED.

Ferroptosis is a recently recognized form of cell death, characterized by intracellular iron accumulation and lipid peroxidation, which disrupts cell membrane integrity. This process has been implicated in a range of diseases, including neurodegenerative disorders, cancer, and cardiovascular conditions.^{5–7} Additionally, ferritin accumulation has been shown to play a critical role in the pathophysiology and progression of diabetes mellitus (DM) and its complications.^{8–10} However, the role of ferroptosis in DMED has not been fully investigated.

The nuclear factor E2-related factor 2 (Nrf2)/heme oxygenase-1 (HO-1) signaling pathway is essential for cellular defense against oxidative stress.¹¹ Nrf2 is a transcription factor that controls the expression of antioxidant enzymes and protective proteins. In response to oxidative stress, Nrf2 dissociates from its repressor Keap1, translocates to the nucleus, and promotes the transcription of genes involved in cellular defense against oxidative damage.¹² HO-1, as a downstream target gene of Nrf2, has antioxidant, anti-inflammatory and cytoprotective functions.¹³ Studies have shown that the flavonoid quercetin can inhibit ferroptosis through the Nrf2/HO-1 signaling pathway, thereby attenuating cerebral ischemic injury.¹⁴ Icarin promotes Nrf2 release by competing with Nrf2 for binding to Keap1, and inhibits oxidative stress, apoptosis and ferroptosis to ameliorate premature ovarian aging.¹⁵ Therefore, whether activation of the Nrf2/HO-1 signaling pathway could help to alleviate oxidative stress and ferroptosis caused by diabetes deserves further investigation.

Currently, first-line treatments for DMED mainly involve phosphodiesterase type 5 (PDE5) inhibitors, including sildenafil. However, nearly 50% of patients do not respond to PDE5 inhibitors,¹⁶ and experience side effects, such as headaches, musculoskeletal pain, and flushing, underscoring the need for alternative treatment options. The flavonoid Icariside II (ICA II), an active ingredient derived from the traditional Chinese medicine Epimedium, exhibits a wide range of biological activities, including antioxidant, anti-inflammatory, anticancer, and neuroprotective effects. Significant progress has been reported in studying ICA II's roles in cardiovascular diseases and neuroprotection.¹⁷ For instance, studies have shown that ICA II reduces myocardial and cerebral ischemia-reperfusion injuries by modulating oxidative stress and inflammation.¹⁸ In recent years, the potential of ICA II in addressing diabetic complications has garnered increasing attention.¹⁹ Wang et al pre-treated DMED with a combination of ICA II and insulin, showing that while insulin effectively controlled blood glucose levels, it was insufficient to fully reverse the pathological changes in erectile tissue. The therapeutic outcomes could be improved by combining strict glycemic control with the antioxidant ICA II to mitigate metabolic memory effects.²⁰

In recent years, researchers have gradually shifted their focus toward the development of derivatives to enhance their bioactivity and therapeutic efficacy. Considering the limited herbal sources of Epimedium, the high extraction costs, and the poor systemic absorption of Icariside (ICA) and ICA II,²¹ their application in clinical settings remains restricted. To address this issue, Gu et al synthesized YS-10, a novel flavonoid derivative of ICA II, through structural optimization of ICA II ([Supplementary Figure 1](#)). This compound not only retains the core structure of 8-prenylkaempferol flavonoids but is also more cost-effective compared to ICA II extracted from plant isolates, while exhibiting excellent biocompatibility and bioactivity.²² In our previous studies, both YS-10 and ICA II were found to effectively improve ED in rats caused by radiation-induced injuries.²³ However, the comparative therapeutic efficacy of YS-10 and ICA II, as well as their underlying mechanisms in DMED, remain unclear. Therefore, in this study, we analyzed and compared the therapeutic effects of ICA II and YS-10 in a rat model of DMED, and explored the mechanistic studies of YS-10 for the treatment of DMED rats, with the aim of providing a conceptual basis for the treatment of DMED and the development of innovative drugs.

Materials and Methods

Animals and Establishment of ED Model

Thirty-six 8-week-old male Sprague-Dawley rats were obtained from Liaoning Changsheng Biotechnology Co., Ltd. (Liaoning, China; animal license number SCXK (Liao) 2020–0001) and housed at the Animal Center of Changchun University of Chinese Medicine. The study was approved by the university's Animal Ethics Committee (Approval No. 2025136). All animals were housed in metabolic cages under standard conditions with a 12-hour light/dark cycle, controlled room temperature, and free access to food and water. In addition, we followed the National Institutes of Health (NIH) Guide for the Care and Use of Laboratory Animals, the ARRIVE guidelines, and the “Laboratory Animal—Guideline for Ethical Review of Animal Welfare (GB/T 35892–2018)” issued by the General Administration of Quality Supervision, Inspection and Quarantine of the People's Republic of China and the Standardization Administration of China to ensure the welfare of the laboratory animals. These guidelines were strictly adhered to throughout the study, ensuring all procedures complied with ethical standards.

For type 1 diabetes mellitus (T1DM) induction, streptozotocin (STZ, 60 mg/kg; Sigma-Aldrich) was diluted in citrate phosphate buffer (0.1 mol/L, pH 4.5) and administered intraperitoneally to thirty rats, as previously described.^{24–26} Six control rats were given citrate phosphate buffer only. Blood glucose and body weight were monitored daily, and rats with blood glucose levels exceeding 16.67 mmol/L for three consecutive days, along with signs of polyuria, polydipsia, and polyphagia, were classified as diabetic. After four weeks, five model group rats died, leaving twenty-five diabetic rats and six normal rats remaining in the study.

Eight weeks post-modeling, apomorphine (APO, 80 mg/kg; Sigma-Aldrich, USA) in 0.1 g/L saline was administered to the diabetic rats. A total of eighteen APO-negative rats were ultimately selected for subsequent experiments and were classified as the DMED model. Subsequently, these SD rats were further divided into 3 groups: the DMED group (n = 6), the DMED + ICA II group (n = 6), the DMED + YS-10 group (n = 6). And the control group (n = 6), totaling twenty-four rats for subsequent experiments. Of these, the DMED + ICA II and DMED + YS-10 groups received daily gavage (2.5 mg/kg/day),^{22,23} whereas the DMED and control groups received an equivalent volume of solvent (saline). Intragastric administration was performed daily for 4 weeks. A 3-day washout period was introduced after treatment to exclude any acute effects of the final dose and to better reflect the treatment's sustained biological impact.^{22,27} Erectile function was subsequently assessed in all rats, and penile tissues were collected for further analysis (Figure 1A).

Erectile Function Evaluation

Erectile function was assessed after 4 weeks of treatment in each group of rats, following established protocols.^{25,28,29} Briefly, SD rats were anesthetized with a 30 mg/kg intraperitoneal injection of 5% sodium pentobarbital. The rats were positioned supine, and a “V-shaped” incision was made in the carotid artery using micro-scissors. PE-50 tubing, pre-filled with heparinized saline (200 IU/mL), was inserted, ligated, and connected to a multichannel physiological recorder (MP36R, Biopac Systems, USA) to monitor mean arterial pressure (MAP). The pelvic ganglion was located dorsolaterally to the prostate through a median lower abdominal incision, and the cavernous nerve (CN) was identified. For intracavernous pressure (ICP) measurements, a 24G needle was inserted into the left corpus cavernosum and connected to the MP36R via PE-50 tubing. The cavernous nerve was stimulated electrically (15 hz, 5.0 V, 1 min) using a bipolar electrode. Erectile function was evaluated by comparing the maximum ICP/MAP ratios across groups. After the assessment, penile tissues were dissected, with half fixed in 4% paraformaldehyde for histology and the remaining stored at –80°C for further analysis.

Masson's Trichrome Staining

Penile tissue was fixed in 4% paraformaldehyde for 48 h, followed by dehydration in a graded ethanol series. The tissue was then embedded in paraffin and sectioned into 5- μ m slices. Masson staining was performed according to the manufacturer's instructions (Servicebio, China). Stained sections were imaged using Olympus Image Viewer, with smooth muscle appearing red and collagen fibers blue. The smooth muscle-to-collagen ratio was analyzed semi-quantitatively using ImageJ software to evaluate collagen deposition in the corpora cavernosa.

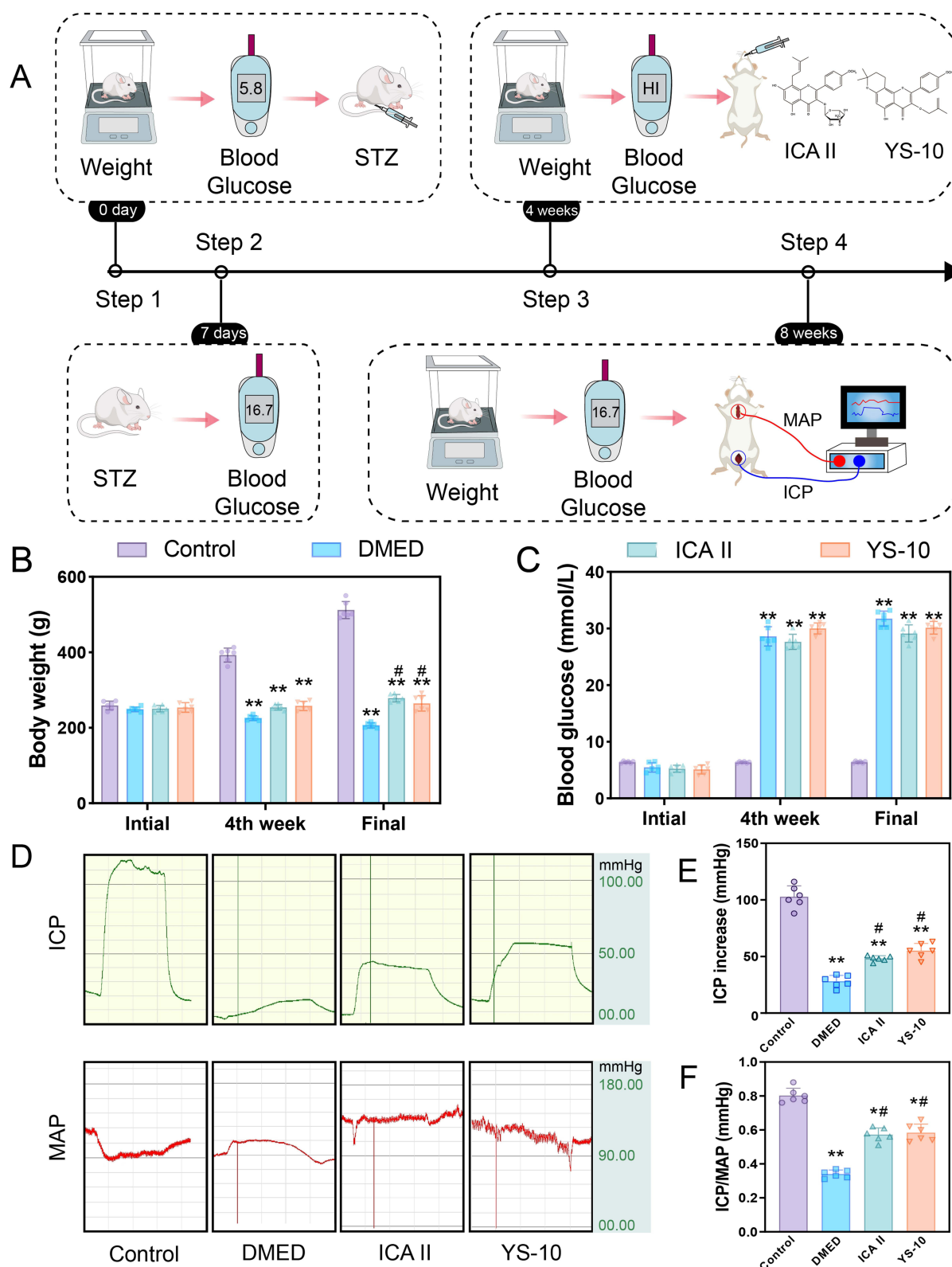


Figure 1 A novel flavonoid derivative of icarisperide II (YS-10) improves erectile function in DMED rats. **(A)** Schematic diagram of the animal experimental process. **(B)** Changes in body weight of rats in each group during the experiment. **(C)** Changes in blood glucose levels of rats in each group during the experimental process. **(D)** Original records of ICP and MAP changes in each group of rats under electrical stimulation. **(E and F)** Statistical analysis of ICP and ICP/MAP in each group of rats. (*, $p < 0.05$ compared with Control group; **, $p < 0.01$ compared with Control group; #, $p < 0.05$ compared with DMED group; ##, $p < 0.01$ compared with DMED group. ICP: intracavernous pressure; MAP: mean arterial pressure).

Detection of Reactive Oxygen Species (ROS) Generation

Dihydroethidium (DHE) staining solution was prepared and diluted according to the manufacturer's instructions (Beyotime, S0063), and applied to the frozen tissue sections. After a 30-min incubation at room temperature in the dark, the sections were washed with PBS to remove excess DHE and then mounted with an anti-fluorescence quenching agent. Red fluorescence was observed and captured using a fluorescence microscope to assess ROS levels.

Oxidative Stress Indicator Test

Penile tissue was homogenized in an ice bath to prepare a 10% tissue homogenate, which was then centrifuged at 4000 rpm for 10 min at 4°C. The supernatant was collected for analysis of superoxide dismutase (SOD), catalase (CAT), glutathione peroxidase (GSH-Px), thiobarbituric acid reactive substances (TBARS), lipid peroxidation (LPO), and malondialdehyde (MDA) levels. These markers were used to assess oxidative and antioxidant activity in the penile tissues. All reagents were sourced from Beyotime, and the assay was conducted following the manufacturer's protocol.

Assessment of Iron Content

Iron content in the sponge tissues was measured using the tissue iron assay kit (A039-2-1, Nanjing Jianjian Bioengineering Institute, China), following the manufacturer's instructions.

Detection of Inflammatory Factors

After blood collection from the rat tail vein, serum was separated by centrifugation. The levels of TNF- α , IL-1 β , IL-6, and IL-10 in the serum were measured using an ELISA kit (Yanko Biotech, Huangshi, China), following the manufacturer's protocol.

Immunohistochemical Staining of Animal Tissues

In this experiment, we used immunohistochemical and immunofluorescence methods to detect Glutathione peroxidase 4 (GPX4) and acid acyltransferase 4 (ACSL4) in the penile cavernous tissue of each group. Penile cavernous tissue samples were collected, rinsed with saline, and fixed in 4% paraformaldehyde for 30 min. After fixation, the tissues were sectioned into 5- μ m slices and subjected to antigen retrieval. The sections were blocked with 5% BSA for 1 hour to reduce nonspecific binding, then incubated overnight at 4°C with primary antibodies against GPX4 (1:200, #DF6701, Affinity) and ACSL4 (1:200, #DF12141, Affinity). After primary antibody incubation, the sections were treated with an appropriate secondary antibody for 1 hour. DAB was used for color development, followed by counterstaining, mounting, and imaging under a microscope. For immunofluorescence, fluorescently labeled secondary antibodies were applied, washed, and mounted with an anti-fade mounting medium. Finally, the fluorescence signal and distribution were observed and recorded using a microscope.

Cell Culture

CCECs were purchased from Saibaikang Biotechnology Co., China, and cultured in DMEM supplemented with 10% fetal bovine serum (FBS) and 1% penicillin-streptomycin. Cells were maintained at 37°C in a 5% CO₂ incubator, with subculturing every 2–3 days to maintain optimal growth conditions. Subsequent experiments were carried out after the cells were stabilized and expanded to the third passage.

Cell Modeling and Cell Viability Assays

Cell proliferation was assessed using the Cell Counting Kit-8 (CCK-8, C0042, Beyotime, China). Cells were seeded at a density of 1×10^5 cells per well in 96-well plates and allowed to adhere for 24 h. Afterward, they were treated with varying concentrations of AGEs (0–300 μ g/mL), and 10 μ L of CCK-8 solution was added to each well after 1 hour of incubation at 37°C. Absorbance was measured at 450 nm using a microplate reader to determine the optimal AGE concentration. The same assay was used to determine the optimal concentrations of the ferroptosis inhibitor (Fer-1, HY-100579), ferroptosis inducer (Erastin, Era, HY-15763), antioxidant (Trolox, HY-101445), Nrf2 inhibitor (ML385, MCE), and YS-10.

Cell Model Grouping

When the cells achieved stable growth, they were allocated into experimental groups: control group (Control), AGEs induction model group (AGEs, 250 $\mu\text{g}/\text{mL}$), ferroptosis agonist group (Erastin, 3 μM), YS-10 administration group (50 μM), ferroptosis inhibitor group (Fer-1, 2 μM), and Nrf2 inhibitor group (ML385, 5 μM).³⁰ All groups were utilized for subsequent experimental analysis.

Assessment of Cellular Lipid ROS Production

To detect lipid ROS production at the cellular level, the culture medium was removed from treated cell slides, and cells were washed 2–3 times with PBS. After fixation in 4% paraformaldehyde for 15 min, the slides were rinsed again with PBS. A hydrophobic barrier pen was used to outline the tissue, and a 1:1000 dilution of BODIPY working solution (GLPBIO, GC42959) was applied to the slides. The samples were incubated for 1 hour at 37°C, protected from light (with water added to the wet box to prevent evaporation). After staining, the slides were washed three times with PBS (pH 7.4) for 5 min each, followed by DAPI staining for 10 min at room temperature. The slides were then washed again, air-dried, sealed with an anti-fluorescence quenching agent, and examined under a fluorescence microscope with image capture.

Immunohistological Staining

In this experiment, GPX4 and ACSL4 in penile corpus cavernosum tissue were visualized using immunohistochemistry and immunofluorescence techniques. First, paraffin sections were cut to 5 μm thick for antigen retrieval. Next, sections were blocked with 5% BSA for 1 hour to minimize non-specific binding, then incubated overnight at 4°C with primary antibodies against GPX4 (1:200, #DF6701, Affinity) and ACSL4 (1:200, #DF12141, Affinity). Following this, the sections were treated with the appropriate secondary antibodies for 1 hour. Immunohistochemistry was performed using DAB staining followed by counterstaining and mounting, and immunofluorescence was performed using fluorescently labeled secondary antibodies, washed, and mounted with an anti-fluorescence quenching agent. The fluorescence signal and distribution were observed and recorded under a microscope.

Cells were plated in 6-well plates at a density of 2×10^5 cells per well and incubated at 37°C for 24 h. After fixation with 4% paraformaldehyde for 10 min, the cells were washed with PBS to remove excess fixative. Permeabilization was performed with 0.1% Triton X-100 for 5–10 min at room temperature, followed by PBS washes. A 5% BSA blocking solution was applied and incubated for 1 hour. The cells were then incubated overnight at 4°C with primary antibodies (GPX4, 1:200, #DF6701, Affinity; Nrf2, 1:200, #AF0639, Affinity). After washing to remove unbound antibodies, the cells were incubated with fluorescently labeled secondary antibodies for 1 hour at room temperature. Finally, DAPI was added to stain the nuclei for 10 min, and the cells were observed under a fluorescence microscope to assess treatment effects on cell morphology and structure.

Bioinformatics Research

For molecular docking experiments, the 2D structure of YS-10 was first constructed using ChemDraw software. Next, the 2D structure was imported into ChemDraw 3D software, and energy minimization was performed using the MM2 module to obtain the lowest energy conformation. Subsequently, the structure of the target protein was downloaded from the PDB database and visualized using PyMOL software.

Next, the following steps were performed using MGLTools 1.5.6 software: removal of water molecules, addition of hydrogen atoms, calculation of charges, and incorporation of non-polar hydrogens. Afterwards, molecular docking of the core target and its active components was performed using CB-Dock, an online docking tool powered by the AutoDock Vina kernel. The binding ability of the target proteins to the molecules was assessed by the Vina docking score, and the conformations with higher scores were selected, visualized, and analyzed using Discovery Studio software.

Western Blot

We conducted Western blot analysis to assess protein expression in rat penile tissues and cells across different experimental groups. Approximately 50 mg of frozen penile tissue was homogenized, and RIPA lysis buffer containing protease and phosphatase inhibitors was added to prevent protein degradation. For cell analysis, 5×10^6 cells were collected, washed with PBS, and lysed with lysis buffer. After centrifugation, the supernatant was collected to obtain total protein.

The protein concentration was determined using the BCA assay, and samples were mixed with loading buffer, heated, and subjected to SDS-PAGE for separation. Proteins were then transferred to PVDF membranes, which were blocked with 5% BSA for 1 hour to minimize non-specific binding. The membranes were incubated overnight at 4°C with primary antibodies against GPX4 (1:1000, #DF6701, Affinity), Nrf2 (1:1000, #AF0639, Affinity), HO-1 (1:1000, #AF5393, Affinity), and β -actin (1:1000, #4967, CST). Following incubation, the membranes were probed with secondary antibodies for 1 hour to enhance the signal, and unbound antibodies were washed away.

The results were captured using an infrared imaging system (LI-COR Biosciences), and semi-quantitative analysis was performed with ImageJ software to quantify the grayscale intensity of each band. Protein levels were normalized to β -actin for comparison.

Statistical Analysis

The statistical analysis was performed using GraphPad Prism 9.0. Data were normally distributed and are expressed as mean \pm standard deviation. Group differences were analyzed using one-way ANOVA or unpaired Student's *t*-test, with statistical significance defined as a *p*-value < 0.05 .

Results

YS-10 Effectively Improves Erectile Function in DMED Rats

In this experiment, [Figure 1B](#) and [C](#) presents the body weight and fasting blood glucose data for each group. Prior to modeling, no significant differences were observed in body weight or fasting blood glucose levels between the groups ($p > 0.05$). However, before drug administration and pressure measurements, the rats in the DMED, DMED+ICA II, and DMED+YS-10 groups showed significantly elevated fasting blood glucose and reduced body weight compared to the control group ($p < 0.01$). There were no significant differences in either parameter between the DMED+ICA II and DMED+YS-10 groups ($p > 0.05$).

Following the 3-day elution period, changes in ICP and MAP waveforms were observed and recorded after 5V electrical stimulation of the cavernous nerve ([Figure 1D–F](#)). Statistical analysis revealed no significant differences in MAP between groups. However, the maximum ICP/MAP ratio in the DMED group was significantly lower than that in the control group ($p < 0.05$), indicating severe erectile dysfunction. In contrast, the DMED+ICA II and DMED+YS-10 groups exhibited significantly higher maximum ICP/MAP ratios compared to the DMED group ($p < 0.05$), with no significant difference between these two groups ($p > 0.05$), suggesting that both ICA II and YS-10 effectively improved erectile function in DMED rats.

YS-10 Ameliorates Histopathological Damage to the Cavernous Body of the Rat Penis

In this experiment, we used Masson staining to evaluate the extent of damage in the penile corpus cavernosum ([Figure 2A](#) and [B](#)). The results showed that the collagen fibers of the corpus cavernosum were significantly increased in the DMED group, and the degree of fibrosis was significantly higher compared with the Control group ($p < 0.05$), indicating that diabetic conditions result in significant structural damage to the corpus cavernosum. After YS-10 treatment, the collagen level was significantly reduced and was not statistically different from the ICA II group ($p > 0.05$).

In addition, we performed α -SMA immunohistochemical staining ([Figure 2C](#) and [D](#)) on different groups. The results showed that the Control group had a uniform distribution of α -SMA-positive cells, displaying a normal smooth muscle fiber structure with moderate cell density and intact tissue architecture. In the DMED group, a significant increase in the

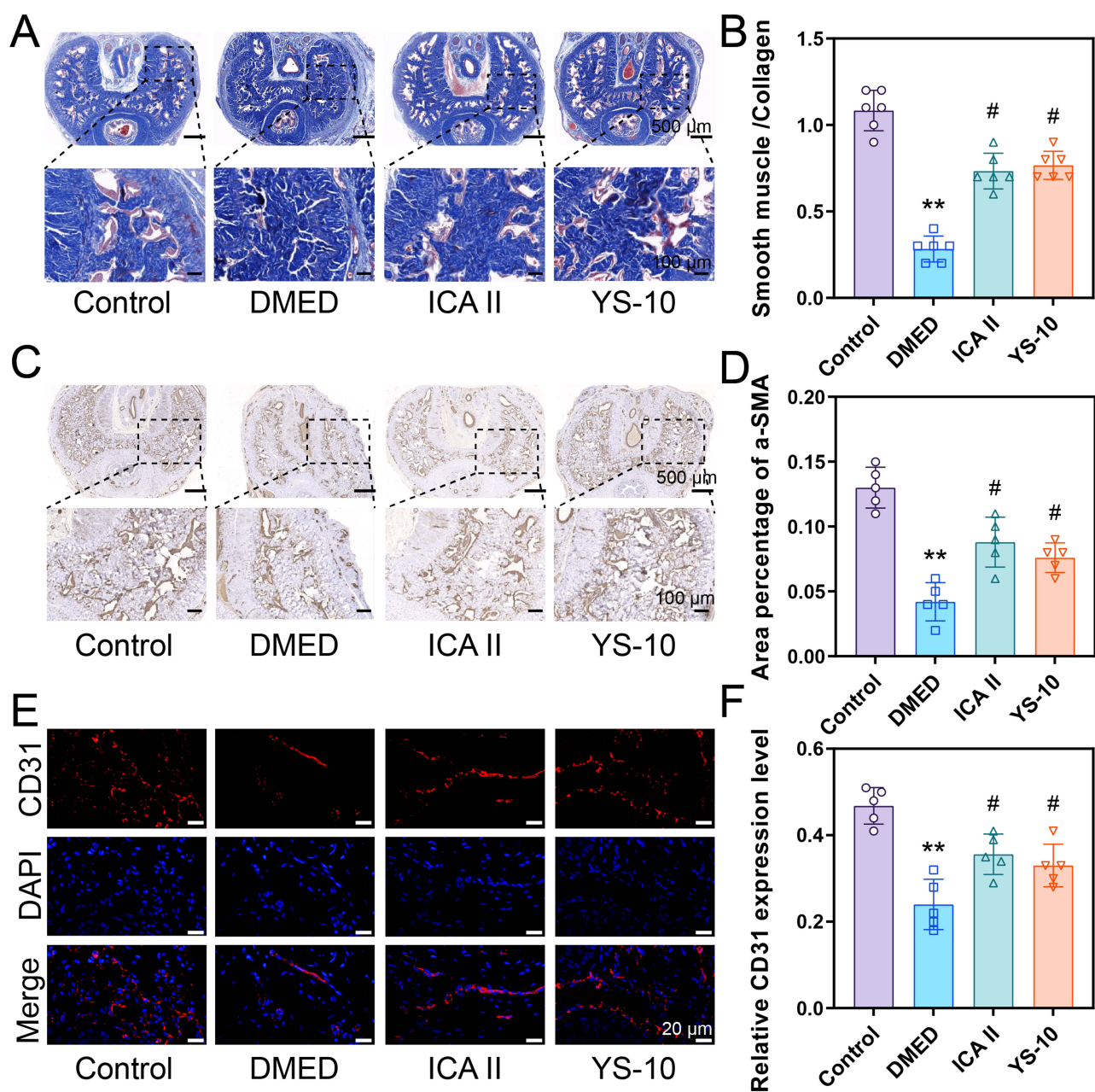


Figure 2 YS-10 repair of penile pathologic injury in DMED rats. **(A and B)** Typical images of Masson trichrome staining of rats in each group and corresponding statistical analysis. Smooth muscle is red and collagen is blue. **(C)** Immunohistochemical staining of α -SMA expression in rats of each group and **(D)** statistical analysis of α -SMA expression. **(E)** Immunofluorescence staining of endothelial cells of rat penile tissue in each group and **(F)** corresponding statistical analysis. (**, $p < 0.01$ compared with the Control group; #, $p < 0.05$ compared with the DMED group).

number of α -SMA-positive cells was observed, along with pronounced cell proliferation, myofibrosis, and irregular tissue architecture, reflecting severe damage. After treatment with ICA II and YS-10, these pathological changes were significantly improved, and approached the level of the Control group ($p < 0.05$).

Finally, immunofluorescence detection of CD31 localization and expression revealed that CD31 was mainly concentrated on the vascular endothelium of the penile corpus cavernosum (Figure 2E and F). Quantitative analysis showed that the fluorescence area and intensity of CD31 in the DMED group were significantly lower than those in the Control group ($p < 0.01$). Compared with the DMED group, the ICA II and YS-10 groups exhibited significant endothelial repair following treatment ($p < 0.05$), with no significant difference between the two groups ($p > 0.05$), and both were close to

normal levels. These results further verified that YS-10 could effectively restore the number of damaged endothelial cells in the penile corpus cavernosum under diabetic conditions.

YS-10 Reduces Oxidative Stress, Inflammation, and Lipid Peroxidation in the Penile Corpus Cavernosum Tissue of Rats

ROS levels in the penile cavernous tissue of each group were measured using a DHE fluorescent probe (Figure 3A and B). The results indicated a significantly larger red fluorescence area in the DMED group compared to the control group ($p < 0.05$), suggesting a strong link between diabetes-induced ED and oxidative stress. Treatment with ICA II and YS-10 significantly reduced the fluorescence area compared to the DMED group ($p < 0.05$), indicating that YS-10 effectively suppressed ROS production.

We also measured oxidative stress markers (Figure 3C–H) by ELISA. The results showed that the levels of SOD, GSH-Px, and CAT were significantly elevated in the control group and markedly reduced in the DMED group ($p < 0.01$). Meanwhile, the levels of MDA, TBARS, and LPO were significantly higher in the DMED group ($p < 0.01$), suggesting that increased oxidative stress led to cavernosal tissue injury. The YS-10 group showed antioxidant marker levels close to those of the control group ($p < 0.01$), while the levels of MDA, TBARS, and LPO were significantly lower, indicating that YS-10 had good efficacy in reducing oxidative injury.

In addition, levels of inflammatory factors IL-1 β , IL-6, and TNF- α were significantly higher in the DMED group compared to the control group ($p < 0.01$), but were markedly reduced in the DMED+ICA II and DMED+YS-10 groups ($p < 0.01$). In contrast, IL-10 expression was significantly elevated in the treatment groups ($p < 0.01$), indicating that YS-10 effectively mitigated inflammation (Figure 3I–L). These findings demonstrate that YS-10 significantly alleviated both oxidative stress and inflammation in the penile corpus cavernosum tissue of DMED rats, with no notable difference from the ICA II group ($p > 0.05$).

YS-10 Reduces the Level of Ferroptosis in the Penile Corpus Cavernosum Tissue of DMED Rats

In this experiment, we found that treatment with ICA II and YS-10 significantly improved the iron content in the DMED group (Figure 3M). Therefore, we further examined the expression levels of GPX4 and ACSL4 in penile corpus cavernosum tissues of different experimental groups by immunohistochemistry and immunofluorescence to assess the effects of ICA II and YS-10 on ferroptosis. Immunohistochemical results showed (Figure 4A) that ACSL4 expression was lower in the control group and significantly higher in the DMED group ($p < 0.01$), indicating significant ferroptosis. Meanwhile, ACSL4 expression was significantly lower in the ICA II and YS-10 groups ($p < 0.01$), and there was no statistically significant difference between the two ($p > 0.05$), verifying the inhibitory effect of YS-10 on ferroptosis.

Meanwhile, the control group showed higher GPX4 expression levels and uniform cell staining, highlighting its role in maintaining antioxidant capacity. In contrast, GPX4 expression in the DMED group was significantly lower ($p < 0.01$), suggesting an increased risk of ferroptosis. The expressions of GPX4 in the ICA II and YS-10 groups were significantly higher compared to the DMED group ($p < 0.05$), and approached the level of the control group ($p > 0.05$), indicating that YS-10 effectively attenuated ferroptosis.

In addition, the immunofluorescence results of GPX4 further supported this finding (Figure 4B). These results suggest (Figure 4C–E) that YS-10 may protect the penile corpus cavernosum by enhancing the expression of GPX4 and inhibiting the expression of ACSL4, thereby offering insights into the link between ferroptosis and penile dysfunction.

YS-10 Can Improve Oxidative Stress and Ferroptosis Induced by AGEs in CCECs

To determine the optimal concentration for modeling CCECs, cells were treated with varying concentrations of AGEs, and cell viability was assessed using the CCK-8 assay. The results showed a significant reduction in cell viability at 24 h with 250 $\mu\text{g/mL}$ of AGEs, compared to the control group ($p < 0.05$), with further decreases observed at higher concentrations. Based on these findings, subsequent experiments used AGEs at a concentration of 250 $\mu\text{g/mL}$. (Figure 5A).

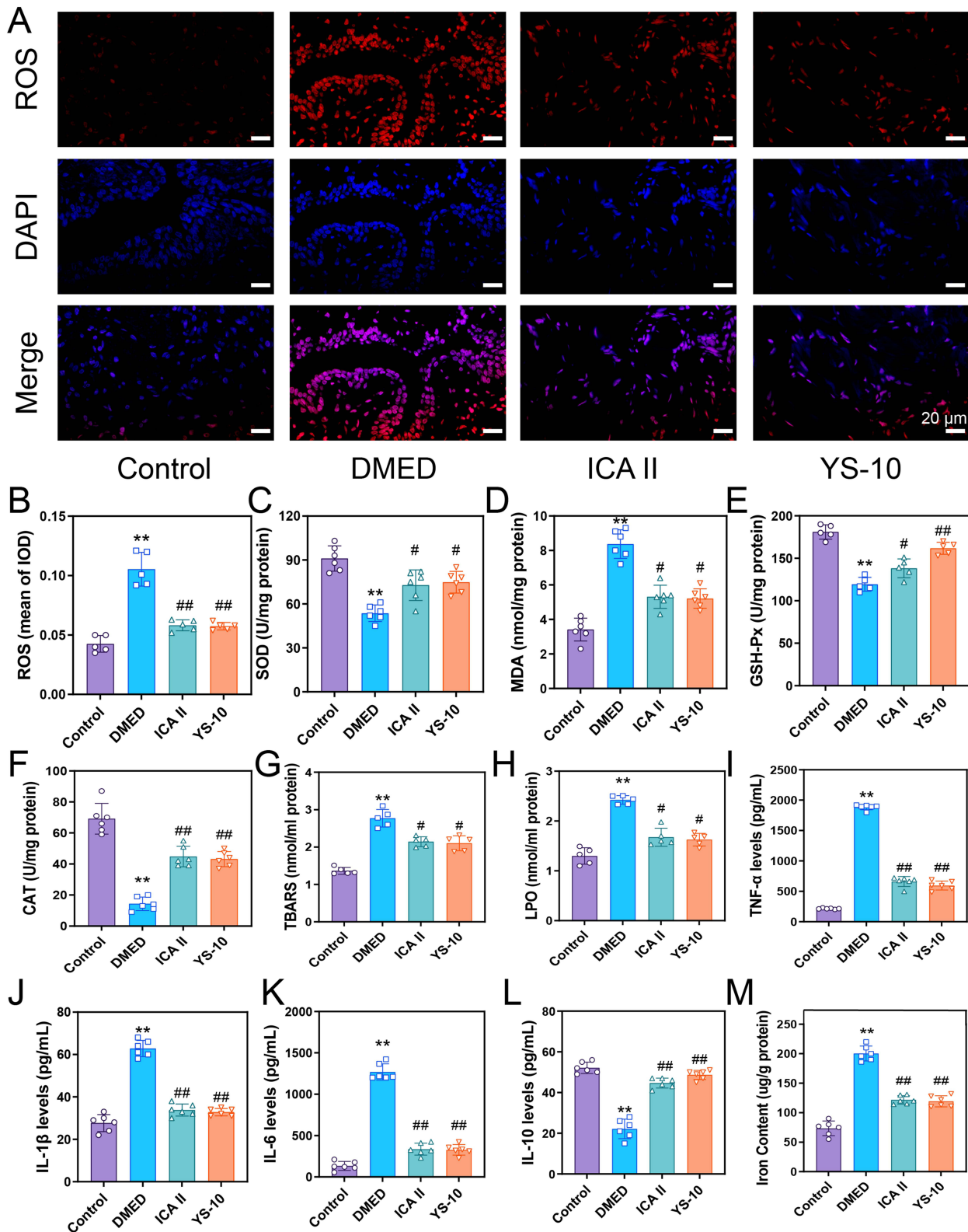


Figure 3 YS-10 improves DMED by modulating oxidative stress and inflammatory responses. **(A)** ROS fluorescence imaging of penile cavernous tissue in each group (scale bar = 20 μm) and **(B)** statistical analysis of the mean fluorescence area of ROS in penile cavernous tissue in each group. **(C-M)** Expression levels of SOD, MDA, GSH-Px, CAT, TBARS, LPO, TNF-α, IL-1β, IL-6, IL-10, and Iron Content in the penises of rats in each group. (**, $p < 0.01$ compared with the Control group; #, $p < 0.05$ compared with the DMED group; ##, $p < 0.01$ compared with the DMED group).

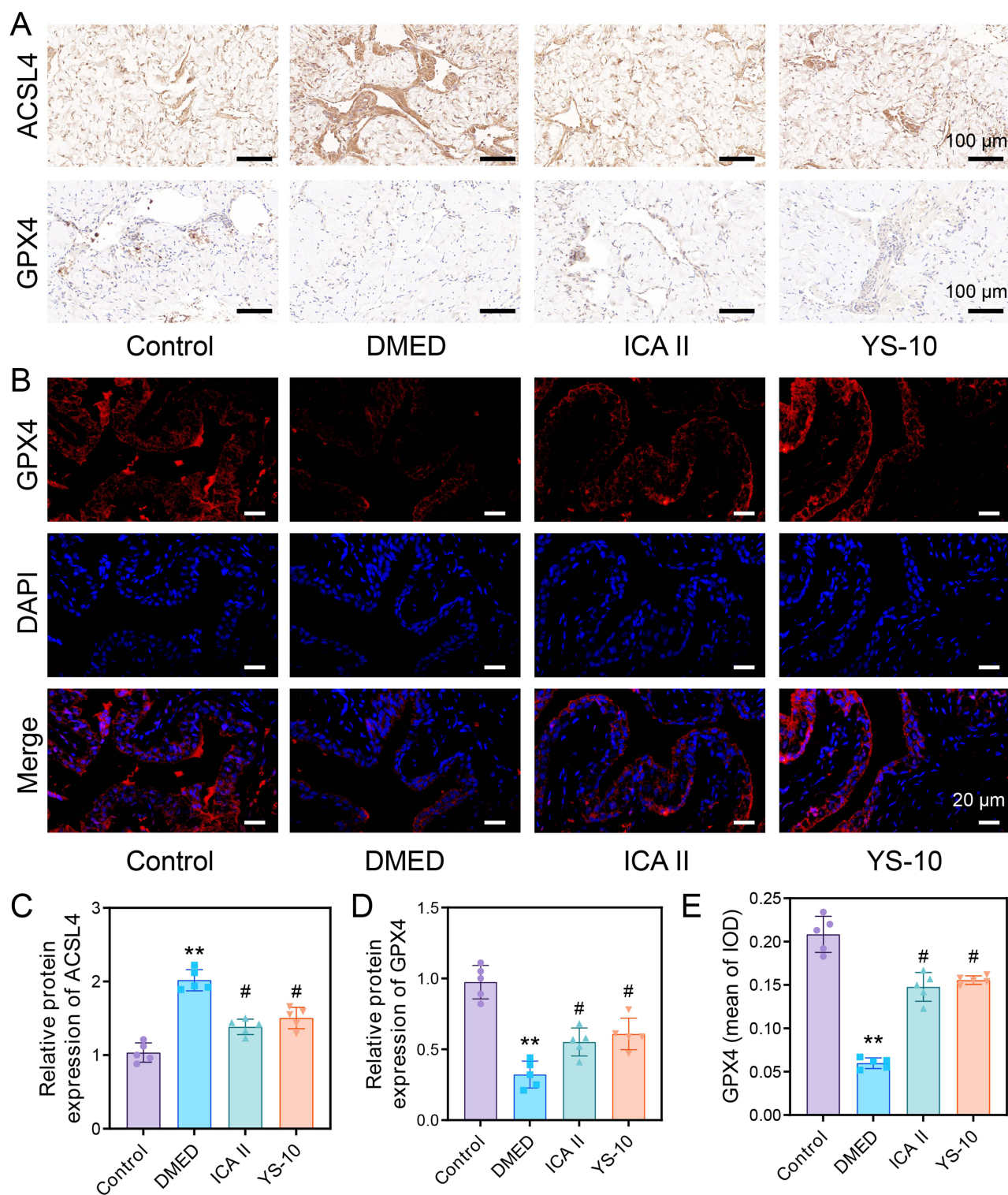


Figure 4 YS-10 ameliorates DMED by inhibiting ferroptosis. **(A)** Representative results of ACSL4 and GPX4 relative expression assessed by immunohistochemistry (IHC). **(B)** Representative results of GPX4 relative expression assessed by immunofluorescence (IF). **(C-E)** Statistical analysis of the results of ACSL4 and GPX4 relative expression assessed by IHC and IF. (**, $p < 0.01$ compared with the control group; #, $p < 0.05$ compared with the ICA II group).

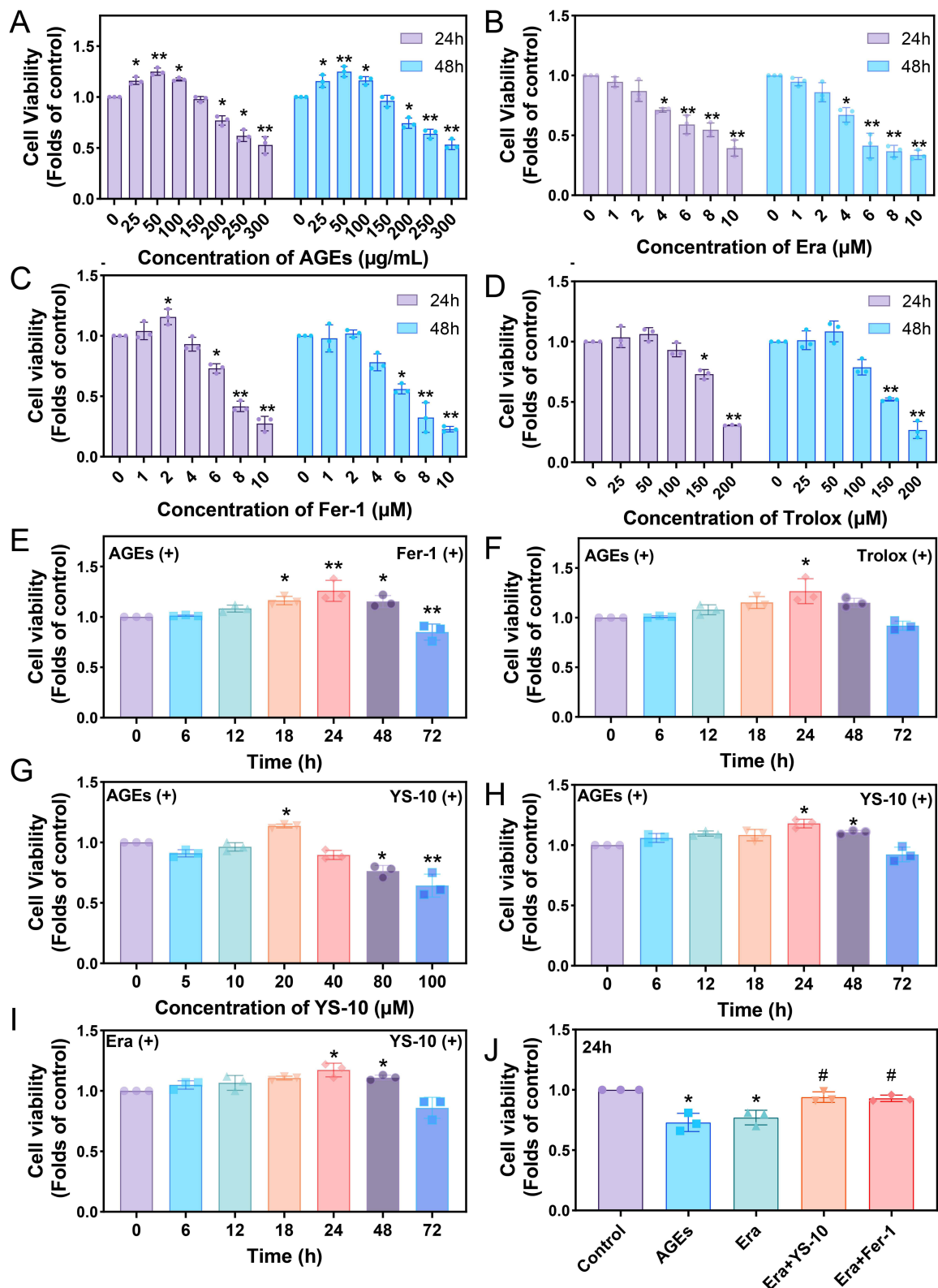


Figure 5 AGEs can induce ferroptosis in CCECs. **(A and B)** Optimal concentrations of AGEs and Erastin for inducing damage to CCECs at 24 and 48h. **(C and D)** Effects of Fer-1 (2 μM, ferroptosis inhibitor) and Trolox (50 μM, antioxidant) on the proliferation of CCECs at 24 and 48h. **(E)** Evaluation of the repairing effect of 2 μM Fer-1 and **(F)** 50 μM Trolox on 250 μg/mL AGEs-induced damage to CCECs at different time points. **(G)** At 24 h, the concentration of YS-10 was adjusted to determine the optimal therapeutic concentration for AGEs-inducible CCECs. By CCK-8 cell viability assay, YS-10 was found to be cytoprotective against CCECs at a concentration of 20 μM. **(H)** Effects of 20 μM YS-10 on CCECs induced by 250 μg/mL AGEs; **(I)** Effects of 20 μM YS-10 on CCECs induced by 4 μM Era at different time intervals. **(J)** Proliferation of CCECs under different factor treatments. (*, $p < 0.05$ compared with the control group; **, $p < 0.01$ compared with the control group; #, $p < 0.05$ compared with the AGEs group).

In addition, the concentration of the ferroptosis agonist Erastin was determined in this study to explore its mechanism. The experimental results showed that 4 μM Erastin significantly reduced cell viability within 24 h compared to the control group ($p < 0.05$) and exhibited a dose-dependent effect (Figure 5B). Using the CCK-8 assay, we further evaluated the protective effects of the ferroptosis inhibitor Fer-1 and the potent antioxidant Trolox on CCECs. (Figure 5C and D). The results showed that when cells were treated with 2 μM Fer-1 and 50 μM Trolox for 24 h, these inhibitors significantly reversed AGEs treatment and Erastin-induced death of CCECs ($p < 0.05$), providing preliminary evidence that ferroptosis and oxidative stress are the primary mechanisms underlying cell death.

To assess the protective effect of YS-10 on CCECs under AGEs treatment, this study optimized the concentration of YS-10 and the duration of the intervention. The CCK-8 cell viability assay showed that YS-10 at 20 μM had a protective effect on CCECs, with its protective effect peaking at 24 h of treatment (Figure 5G and H). However, prolonged exposure or higher concentrations of YS-10 did not enhance the protective effect, but instead reduced it, indicating a dose- and time-dependent response.

To evaluate the potential of YS-10 in reversing ferroptosis in CCECs, ferroptosis was induced by treating the cells with 4 μM Erastin, while 20 μM YS-10 was administered at the time of induction. Cell viability was monitored at multiple time points. The results indicated that the highest cell activity was observed at 24 hours (Figure 5I). Furthermore, YS-10 not only reversed Erastin-induced ferroptosis in CCECs, but its effects were also found to be time-dependent, showing a pattern similar to that of the ferroptosis inhibitor Fer-1 (Figure 5J). These findings suggest that YS-10 effectively mitigates Erastin-induced ferroptosis in CCECs, demonstrating its potential as a therapeutic agent in ferroptosis-related conditions.

Next, we further evaluated the protective effects of YS-10 on AGEs-induced oxidative stress and ferroptosis in CCECs using immunofluorescence (Figure 6A). The results showed a significant increase in ROS and Lipid ROS expression in the AGEs group, indicating that AGEs induced oxidative stress, which was not observed in the control group. In contrast, ROS and Lipid ROS levels were significantly lower in the YS-10 and Fer-1 treatment groups, suggesting that both YS-10 and Fer-1 effectively reduced AGEs-induced oxidative stress, with no significant difference between the two treatments ($p > 0.05$).

Regarding ferroptosis-related markers (Figure 6B and C), both the AGEs and Erastin groups exhibited a significant increase in ACSL4 levels and a marked decrease in GPX4 expression, indicating that both AGEs and ferroptosis-inducing agents similarly trigger ferroptosis. The YS-10 treatment group showed a significant decrease in the level of ACSL4, along with a significant increase in the level of GPX4, further demonstrating the potential of YS-10 in inhibiting ferroptosis. The Fer-1 group exhibited effects similar to YS-10, showing the effectiveness of Fer-1 in decreasing the expression of ACSL4 and increasing the expression of GPX4.

In addition, the ELISA assay showed that MDA levels were significantly higher and GSH levels were significantly lower in the AGEs group, further validating the presence of oxidative stress (Figure 6D and E). Notably, MDA levels were significantly decreased and GSH levels were restored to near-normal levels in both the YS-10 treatment group and the Fer-1 group, suggesting that both YS-10 and Fer-1 were effective in ameliorating AGEs-induced oxidative stress injury.

In summary, AGEs-induced oxidative stress and ferroptosis resulted in significant cellular damage in CCECs, and both YS-10 and Fer-1, a ferroptosis inhibitor, were effective in mitigating these damages. This suggests that the protective effect of YS-10 may be related to its mechanism of inhibiting ferroptosis and ameliorating oxidative stress.

YS-10 Induces Ferroptosis Response in CCECs in Association with the Nrf2/HO-1/ GPX4 Signalling Pathway

The expression of Nrf2/HO-1 proteins has been recognized as a key regulator of ferroptosis.³¹ Therefore, we investigated whether YS-10 could mitigate AGEs- and Erastin-induced ferroptosis damage through the Nrf2/HO-1 signalling pathway. First, we analysed the schematic of the monomeric structure of YS-10 (Figure 7A) and performed molecular docking with Nrf2, HO-1, and GPX4 (Figure 7B). The docking visualisation results showed that YS-10 was tightly bound to Nrf2, HO-1, and GPX4 through hydrogen bonding and hydrophobic interactions, with minimum binding

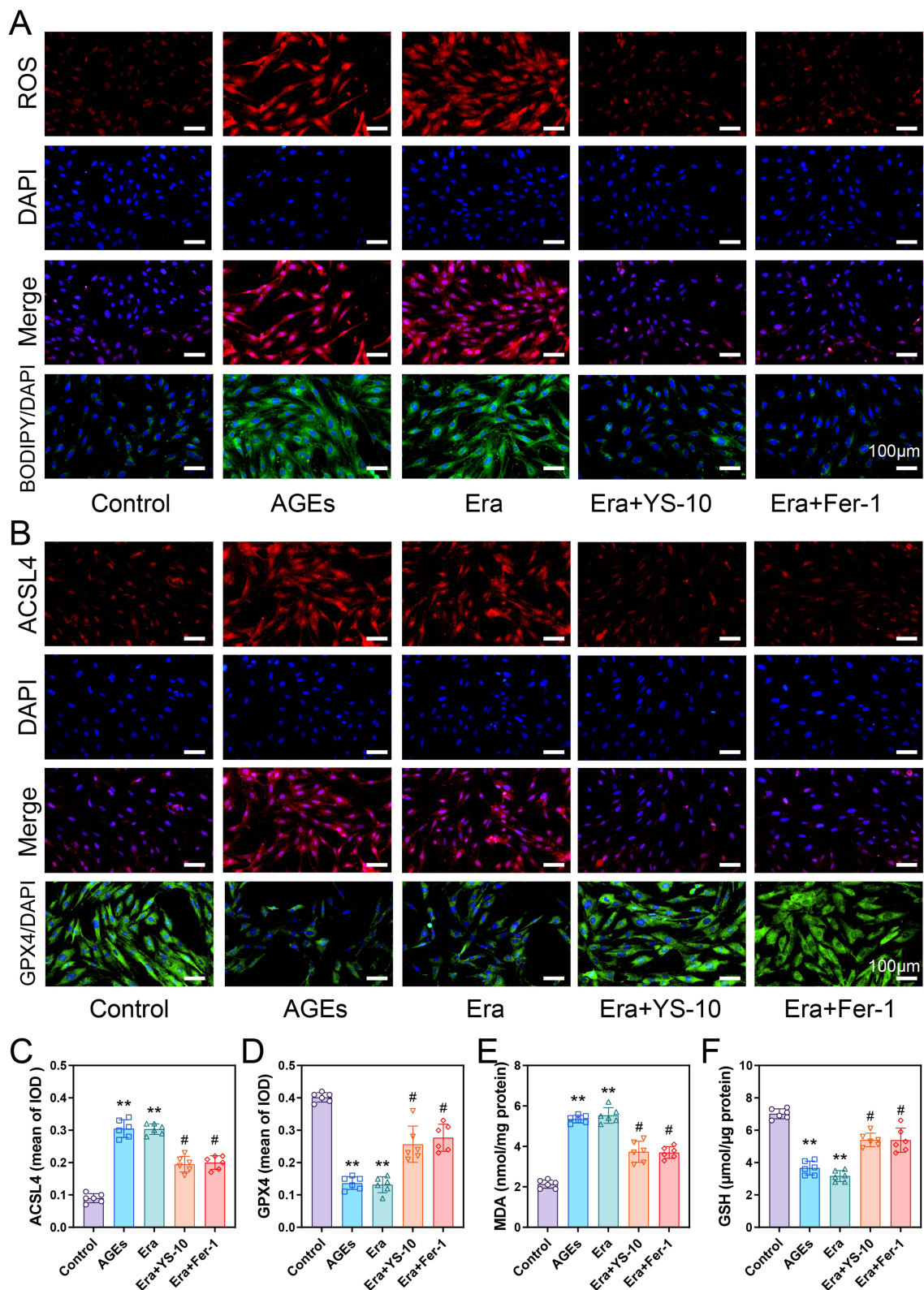


Figure 6 YS-10 has ameliorative effects on AGEs-induced oxidative stress and ferroptosis in CCECs. **(A)** Characteristic images of the expression levels of ROS and Lipid ROS in different subgroups among CCECs cells. **(B)** Characteristic images of the index changes of ferroptosis markers ACSL4 and GPX4 in different subgroups and **(C and D)** corresponding statistical analyses. **(E and F)** Elisa assay of the trend levels of changes in oxidative stress indicators MDA as well as GSH at the cellular level. (**, $p < 0.01$ compared with the control group; #, $p < 0.05$ compared with the AGEs group).

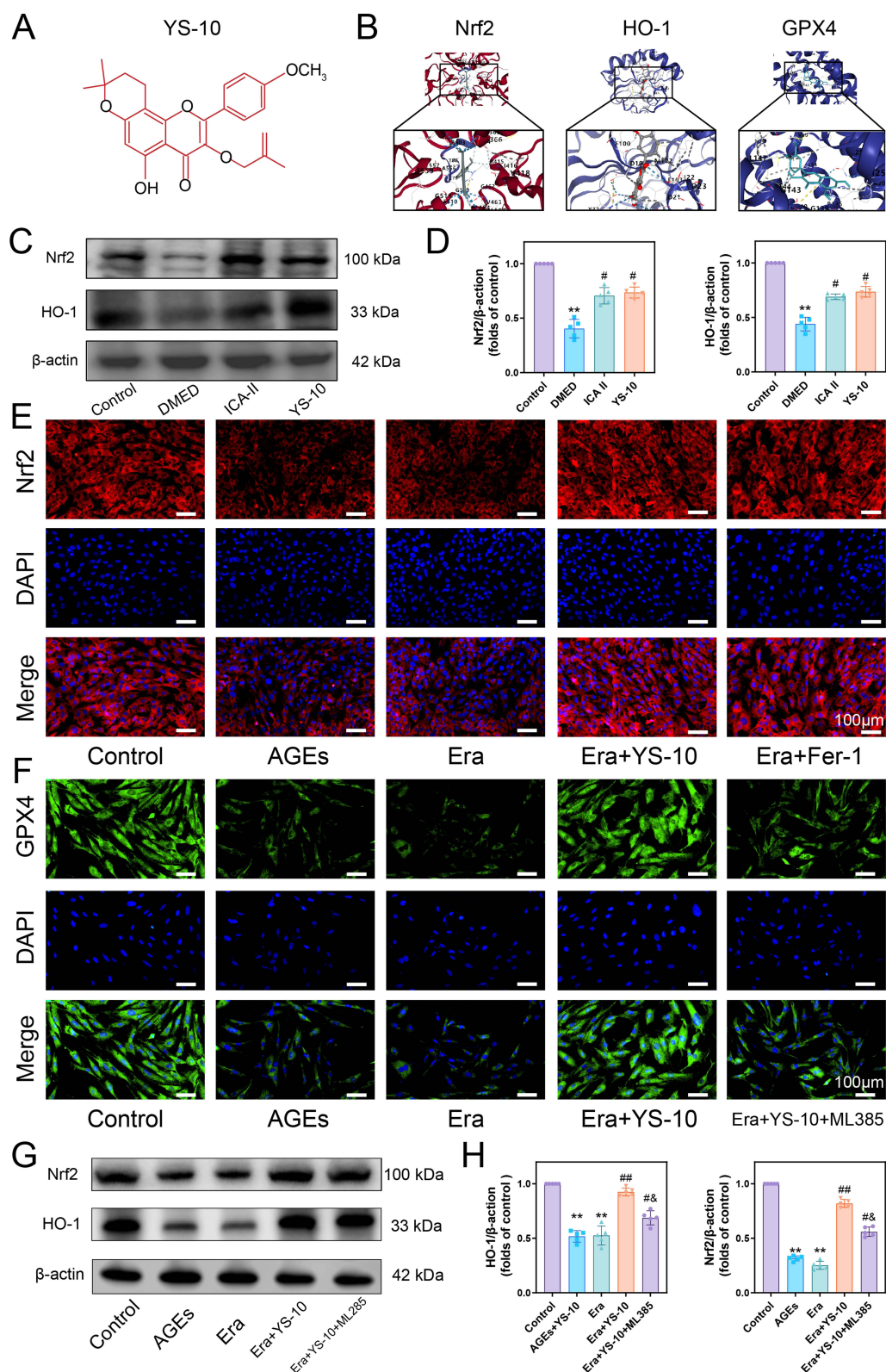


Figure 7 YS-10 regulates ferroptosis to improve endothelial cell recovery through Nrf2/HO-1/GPX4 signaling pathway. **(A)** Monomer structural formula of YS-10. **(B)** Molecular docking visualization results of YS-10 with Nrf2, GPX4 and HO-1. **(C and D)** Expression levels of Nrf2 and HO-1 in the penile tissues of different subgroups of rats, and the corresponding statistical analysis (**, $p < 0.01$ compared with the control group; #, $p < 0.05$ compared with the DMED group). **(E)** Characteristic images of Nrf2 expression in cells of Control, AGEs, Era, Era+YS-10, and Era+Fer-1 groups. **(F)** The ferroptosis indicator GPX4 in Control, AGEs, Era, Era+YS-10, and Era+YS-10+ML385 groups expression levels as well as **(G and H)** protein expression levels of Nrf2 and HO-1 verified by Western blot and their corresponding statistical analyses. (**, $p < 0.01$ compared with the control group; #, $p < 0.05$ compared with the AGEs group; and, $p < 0.05$ compared with the Era+YS-10 group. ML385: Nrf2 inhibitor. Era: Erastin, Ferroptosis inducer).

energies of -9.9 kJ/mol, -8.6 kJ/mol, and -6.4 kJ/mol, respectively. Specifically, Nrf2 formed hydrogen bonding interactions with GLY462, LEU557, ILE559, VAL606, VAL465, and VAL418 in YS-10; HO-1 formed hydrogen bonding interactions with TYR71, HIS150, ALA149, and GLN34; and GPX4 formed hydrogen bonding interactions with MET51, MET34, and ASN210. These docking results indicated that YS-10 has a strong affinity for Nrf2, HO-1, and GPX4, which may enhance antioxidant capacity and regulate relevant signalling pathways.

Subsequently, we assessed the expression levels of Nrf2 and HO-1 in rat penile tissues by Western blot (Figure 7C and D). Both ICA II and YS-10 significantly increased the expression of Nrf2 and HO-1 in penile tissues of diabetic rats compared with the DMED group.

To explore the role of the Nrf2/HO-1 pathway in ferroptosis, CCECs were treated with the ferroptosis inhibitor Fer-1. Immunofluorescence results revealed that Fer-1 upregulated Nrf2 expression and effectively inhibited ferroptosis, showing effects similar to those of YS-10 treatment (Figure 7E). Additionally, YS-10 significantly promoted the nuclear translocation of Nrf2 (Figure 7E).

To further investigate the mechanism of YS-10, we used ML385, a specific Nrf2 inhibitor, to assess its impact on ferroptosis. Immunofluorescence and Western blot analysis demonstrated that ML385 significantly reduced Nrf2 and HO-1 expression compared to the YS-10 group, partially reversing the anti-ferroptosis effects of YS-10 on CCECs (Figure 7F–H). These findings suggest that YS-10's protective effects against ferroptosis are mediated through the activation of the Nrf2/HO-1/GPX4 pathway.

Discussion

DMED is a serious clinical problem that affects the quality of life of a significant proportion of male patients. Recent studies have identified oxidative stress, endothelial dysfunction, and chronic inflammation as major factors contributing to DMED.²⁴ In this study, we investigated the therapeutic effect of a novel flavonoid ICA II derivative, YS-10, in a rat model of DMED and its mechanism. In addition to evaluating efficacy, the *in vivo* safety profiles of ICA II and YS-10 were also considered. Previous studies have shown that ICA II is safe and well-tolerated at 2.5 mg/kg/day and higher doses, without systemic toxicity or organ damage.^{22,32,33} Similarly, our earlier work using YS-10 in a radiation-induced ED model reported no toxic effects or histopathological abnormalities.²³ In this study, no adverse events, mortality, or organ-related abnormalities were observed in any treatment group, supporting the favorable safety of YS-10. These findings validate the selected dosage and highlight the potential for future translational application.

The mechanism of pathological damage to the penile corpus cavernosum in DMED is complex, with oxidative stress playing a key role, marked by an imbalance between the generation and accumulation of ROS.³⁴ In the diabetic state, multiple pro-oxidative metabolic pathways (eg, glycolysis, protein kinase C, and AGEs) are significantly activated, leading to excessive accumulation of ROS in penile corpus cavernosum tissues, thereby triggering oxidative stress.³⁵ Oxidative stress not only directly damages penile corpus cavernosum endothelial cells but also inhibits endothelial nitric oxide synthase (eNOS) activity, reducing NO and cyclic guanosine monophosphate (cGMP) production, which further leads to endothelial dysfunction.²⁴ In addition, oxidative stress may disrupt the normal function of smooth muscle cells via multiple pathways, and excess free radicals can cause LPO of cell membranes, thereby affecting their fluidity and stability. In our study, this process was confirmed by a decrease in the expression of α -SMA, a marker of penile cavernous smooth muscle cells, and a reduction in LPO levels. Diabetes led to a significant reduction in the expression of the endothelial cell marker CD31, indicating impaired number and function of endothelial cells. Meanwhile, the expression of inflammatory factors IL-1 β , IL-6, and TNF- α was elevated in penile tissues of DMED rats, which may serve as an important trigger of oxidative stress.³⁶ Consistent with previous studies, we found that oxidative stress was highly activated in penile corpus cavernosum tissues of diabetic rats, as evidenced by increased levels of ROS and MDA, as well as decreased SOD activity. After YS-10 treatment, these phenomena were reversed, and the results were similar to the effects of ICA II treatment. In the AGEs-induced CCECs assay, ROS and lipid ROS were significantly increased in the AGEs group, suggesting the presence of significant oxidative stress in CCECs, whereas no such damage was observed in the normal endothelial cell group. In contrast, ROS and lipid ROS levels were significantly reduced in the YS-10-treated group and the ferroptosis inhibitor Fer-1 group, indicating that YS-10 effectively attenuated the oxidative

stress induced by AGEs, thereby protecting CCECs and improving the function of the penile corpus cavernosum. These results suggest that YS-10 may ameliorate the pathology of DMED by attenuating oxidative stress.

Ferroptosis has become an emerging area of research in recent years and plays an important role, particularly in metabolic disorders and neurodegenerative diseases.³⁷ It has been established as a novel therapeutic target for diabetes and its complications. In the context of diabetes, ferroptosis may exacerbate cellular damage via intracellular iron ion accumulation and lipid peroxidation. In the present study, we similarly found that Fe^{2+} content as well as LPO expression levels were significantly elevated in DMED rats, which were effectively ameliorated by ICA II treatment, with YS-10 exhibiting similar effects.

GPX4 is an important antioxidant enzyme capable of degrading lipid peroxidation, while fatty ACSL4 promotes ferroptosis in lipid metabolism. *Ex vivo* and *in vivo* studies have shown that YS-10 significantly up-regulated GPX4 and down-regulated ACSL4, indicating its ability to inhibit ferroptosis and preserve the integrity and functionality of penile corpus cavernosum tissue. ELISA results indicated a notable rise in MDA levels and a reduction in GSH levels in the AGEs group, confirming the occurrence of oxidative stress. In contrast, MDA levels were significantly decreased and GSH levels were restored to near-normal levels in the YS-10 and Fer-1 treatment groups, suggesting that YS-10 was effective in ameliorating the oxidative stress damage induced by AGEs. These results further support the potential application of YS-10 in DMED treatment.

The Nrf2 signalling pathway is closely linked to antioxidant production *in vivo* and plays a critical role in regulating various biological processes, such as the cell cycle, immune response, and apoptosis.³⁸ As an important transcription factor in response to oxidative stress, Nrf2 can induce the expression of various antioxidant enzymes. Studies have shown that YS-10 significantly enhanced the antioxidant capacity of cells by facilitating the nuclear translocation of Nrf2 and activating the expression of the downstream target gene HO-1, which is not only a downstream target gene of Nrf2 but also has antioxidant and anti-inflammatory effects. Its up-regulation further enhances cellular resistance to oxidative stress.

Ferroptosis, a form of cell death strongly associated with oxidative stress, can be effectively suppressed by activating the Nrf2/HO-1 signalling pathway, which helps protect cells from damage.³⁹ Several studies have demonstrated that the Nrf2/HO-1 signalling pathway plays an important role in inhibiting ferroptosis and oxidative stress. For example, ICA attenuates hypoxia/reoxygenation-induced ferroptosis in cardiomyocytes through activation of the Nrf2/HO-1 signalling pathway.⁴⁰ Moreover, Probucol has been shown to alleviate oxidative stress in the penile cavernous tissue of diabetic rats and enhance sexual function by activating the Nrf2/HO-1 pathway. Aligning with these findings, our study revealed that YS-10 significantly upregulated the expression of Nrf2 and HO-1 in both cellular and animal models. Notably, the activation of the Nrf2 pathway is strongly associated with its translocation to the nucleus, and our results confirmed that YS-10 promoted the nuclear translocation of Nrf2. In addition, we found that the Nrf2 inhibitor ML385 was able to reverse the regulatory effect of YS-10 on GPX4, which further suggests that the anti-ferroptosis effect of YS-10 is mediated by the Nrf2/HO-1 signalling pathway.

Overall, our study found that YS-10 significantly improved DMED by enhancing the Nrf2/HO-1/GPX4 signalling pathway and inhibiting ferroptosis, which is consistent with the therapeutic effects observed with ICA II. The revelation of this mechanism not only provides a theoretical basis for the clinical application of ICA II and YS-10 but also highlights potential directions for future drug development.

Despite the positive results obtained in this study, certain limitations still exist. Currently, phosphodiesterase 5 inhibitors (PDE5is) remain the primary treatment for ED. Therefore, future randomized controlled trials with adequate sample sizes are needed to compare the efficacy of ICA II and YS-10 with PDE5is, including their potential synergistic effects when combined. While our study focused on the functional activation of the Nrf2/HO-1/GPX4 signaling pathway, we acknowledge that Keap1, a key negative regulator of Nrf2, was not assessed. This represents a limitation in the depth of our mechanistic investigation. Keap1 plays a critical role in Nrf2 activation, and its evaluation will be essential to fully understand the intricate regulation of this pathway. In addition, the upstream signaling pathways affecting Nrf2 expression were not explored in detail in this study. Future studies could investigate the regulation of ferroptosis through the Sirt1/Nrf2/GPX4 or Prdm16/Nrf2/GPX4 pathways, and explore how interactions between other signaling pathways influence ferroptosis.^{41,42} Assessing Keap1 expression and its role in modulating the Nrf2 pathway in the context of DMED will provide a more comprehensive understanding of the therapeutic potential of Nrf2 activation and its broader implications in treating DMED.

Moreover, our future studies should also focus on the potential application of ICA II and YS-10 in other diabetes-related complications, as well as exploring their therapeutic equivalence, to further evaluate their efficacy in a broader range of clinical applications.

Conclusion

In summary, YS-10, a novel flavonoid derivative of ICA II, significantly improved erectile function in diabetic rats by reducing oxidative stress and ferroptosis via activation of the Nrf2/HO-1/GPX4 pathway. At a dose of 2.5 mg/kg/day, YS-10 showed comparable efficacy to ICA II and demonstrated good safety and tolerability. These findings support the potential of YS-10 as a promising candidate for the treatment of diabetic erectile dysfunction and provide a mechanistic basis for further research and development.

Data Sharing Statement

The data supporting the findings of this study are included in the main text.

For additional information, please contact the corresponding author, ensuring compliance with legal and ethical confidentiality requirements.

Acknowledgments

Special thanks to Prof. Zhong-Cheng Xin from the Male Reproductive and Sexual Medicine Department, Department of Urology, The Second Hospital, Tianjin Medical University, Tianjin, China, for his contribution in providing the YS-10 drug and offering research guidance.

This work was supported by the Department of Science and Technology of Jilin Province [YDZJ202301ZYTS138 and YDZJ202401147ZYTS], and the Projects in Health Commission of Jilin Province [2024A082 and 2022JC048].

Author Contributions

All authors have made substantial contributions to the reported work, whether in the conception, study design, execution, data acquisition, analysis, or interpretation, or in a combination of these areas. They participated in drafting, revising, or critically reviewing the article, and approved the final version to be published. All authors have agreed on the journal to which the article has been submitted and agree to be accountable for all aspects of the work. They are responsible for ensuring that questions related to the accuracy or integrity of any part of the work are appropriately addressed.

Disclosure

The authors report no conflicts of interest in this work.

References

1. Acosta-Martinez M, Cabail MZ. The PI3K/Akt pathway in meta-inflammation. *Int J Mol Sci.* 2022;23(23):15330. doi:10.3390/ijms232315330
2. Yuan T, Yang T, Chen H, et al. New insights into oxidative stress and inflammation during diabetes mellitus-accelerated atherosclerosis. *Redox Biol.* 2019;20:247–260. doi:10.1016/j.redox.2018.09.025
3. An Y, Xu B-T, Wan S-R, et al. The role of oxidative stress in diabetes mellitus-induced vascular endothelial dysfunction. *Cardiovasc Diabetol.* 2023;22(1):237. doi:10.1186/s12933-023-01965-7
4. Chen Y, Xiao M, Zhao L, et al. Low-intensity pulsed ultrasound counteracts advanced glycation end products-induced corpus cavernosal endothelial cell dysfunction via activating mitophagy. *Int J Mol Sci.* 2022;23(23):14887. doi:10.3390/ijms232314887
5. Minami JK, Morrow D, Bayley NA, et al. CDKN2A deletion remodels lipid metabolism to prime glioblastoma for ferroptosis. *Cancer Cell.* 2023;41(6):1048–1060.e9. doi:10.1016/j.ccell.2023.05.001
6. Zhu Y, Fujimaki M, Snape L, et al. Loss of WIPI4 in neurodegeneration causes autophagy-independent ferroptosis. *Nat Cell Biol.* 2024;26(4):542–551. doi:10.1038/s41556-024-01373-3
7. Ichihara G, Katsumata Y, Sugiura Y, et al. MRP1-dependent extracellular release of glutathione induces cardiomyocyte ferroptosis after ischemia-reperfusion. *Circ Res.* 2023;133(10):861–876. doi:10.1161/CIRCRESAHA.123.323517
8. Liu P, Zhang Z, Cai Y, et al. Ferroptosis: mechanisms and role in diabetes mellitus and its complications. *Ageing Res Rev.* 2024;94:102201. doi:10.1016/j.arr.2024.102201
9. Wu Y, Huang T, Li X, et al. Retinol dehydrogenase 10 reduction mediated retinol metabolism disorder promotes diabetic cardiomyopathy in male mice. *Nat Commun.* 2023;14(1):1181. doi:10.1038/s41467-023-36837-x

10. Liu C, Sun W, Zhu T, et al. Glia maturation factor- β induces ferroptosis by impairing chaperone-mediated autophagic degradation of ACSL4 in early diabetic retinopathy. *Redox Biol.* 2022;52:102292. doi:10.1016/j.redox.2022.102292
11. Wang H, Yu X, Liu D, et al. VDR activation attenuates renal tubular epithelial cell ferroptosis by regulating Nrf2/HO-1 signaling pathway in diabetic nephropathy. *Adv Sci.* 2023;11(10):2305563.
12. Tu W, Wang H, Li S, et al. The anti-inflammatory and anti-oxidant mechanisms of the Keap1/Nrf2/ARE signaling pathway in chronic diseases. *Aging Dis.* 2019;10(3):637–651. doi:10.14336/AD.2018.0513
13. Sun -Y-Y, Zhu H-J, Zhao R-Y, et al. Remote ischemic conditioning attenuates oxidative stress and inflammation via the Nrf2/HO-1 pathway in MCAO mice. *Redox Biol.* 2023;66:102852. doi:10.1016/j.redox.2023.102852
14. Peng C, Ai Q, Zhao F, et al. Quercetin attenuates cerebral ischemic injury by inhibiting ferroptosis via Nrf2/HO-1 signaling pathway. *Eur J Pharmacol.* 2024;963:176264. doi:10.1016/j.ejphar.2023.176264
15. Li F, Zhu F, Wang S, et al. Icaritin alleviates cisplatin-induced premature ovarian failure by inhibiting ferroptosis through activation of the Nrf2/ARE pathway. *Sci Rep.* 2024;14(1):17318. doi:10.1038/s41598-024-67557-x
16. Walsh TJ, Hotaling JM, Smith A, et al. Men with diabetes may require more aggressive treatment for erectile dysfunction. *Int J Impot Res.* 2014;26(3):112–115. doi:10.1038/ijir.2013.46
17. Gao J, Ma C, Xia D, et al. Icariside II preconditioning evokes robust neuroprotection against ischaemic stroke, by targeting Nrf2 and the OXPHOS/NF- κ B/ferroptosis pathway. *Br J Pharmacol.* 2022;180(3):308–329. doi:10.1111/bph.15961
18. Gao J, Long L, Xu F, et al. Icariside II, a phosphodiesterase 5 inhibitor, attenuates cerebral ischaemia/reperfusion injury by inhibiting glycogen synthase kinase-3 β -mediated activation of autophagy. *Br J Pharmacol.* 2020;177(6):1434–1452. doi:10.1111/bph.14912
19. Jiang W, Ding K, Yue R, et al. Therapeutic effects of icariin and icariside II on diabetes mellitus and its complications. *Crit Rev Food Sci Nutr.* 2023;64(17):5852–5877.
20. Wang L, Xu Y, Li H, et al. Antioxidant icariside II combined with insulin restores erectile function in streptozotocin-induced type 1 diabetic rats. *J Cell Mol Med.* 2015;19(5):960–969. doi:10.1111/jcmm.12480
21. Cheng T, Zhang Y, Zhang T, et al. Comparative pharmacokinetics study of icariin and icariside II in rats. *Molecules.* 2015;20(12):21274–21286. doi:10.3390/molecules201219763
22. Gu SJ, M L, Yuan YM, et al. A novel flavonoid derivative of icariside II improves erectile dysfunction in a rat model of cavernous nerve injury. *Andrology.* 2021;9(6):1893–1901. doi:10.1111/andr.13065
23. Liu Y, Wei Z, Liu S, et al. A flavonoid derivative of icariside II (YS-10) improves erectile dysfunction in radiation-injured rats via oxidative stress pathway. *Transl Andrology Urol.* 2022;11(6):832–841. doi:10.21037/tau-22-376
24. Mao Y, Zha Y, Zang Y, et al. Isorhamnetin improves diabetes-induced erectile dysfunction in rats through activation of the PI3K/AKT/eNOS signaling pathway. *Biomed Pharmacother.* 2024;177:116987. doi:10.1016/j.biopha.2024.116987
25. Pan X, Xing X, Ji Z, et al. Dual-responsive stem cell microspheres modified with BDNF for enhanced neural repair in diabetic erectile dysfunction. *J Control Release.* 2025;379:409–420. doi:10.1016/j.jconrel.2025.01.002
26. Liu Y, Zheng J-Y, Wei Z-T, et al. Therapeutic effect and mechanism of combination therapy with ursolic acid and insulin on diabetic nephropathy in a type 1 diabetic rat model. *Front Pharmacol.* 2022;13:969207. doi:10.3389/fphar.2022.969207
27. Daffy N, Elizondo GM, Perez-Vasquez C. Differential impact of serotonin signaling methylphenidate on young versus adult: insights from behavioral and dorsal raphe nucleus neuronal recordings from freely behaving rats. *Int J Mol Sci.* 2024;25(15):8082. doi:10.3390/ijms25158082
28. Liu Y, Pan X-Y, Zhang -X-X, et al. Role of mechanotransduction mediated by YAP/TAZ in the treatment of neurogenic erectile dysfunction with low-intensity pulsed ultrasound. *Andrology.* 2023;11(7):1514–1527. doi:10.1111/andr.13438
29. Liu Y, Zhang Z, Zhao Z, et al. An easy nanopatch promotes peripheral nerve repair through wireless ultrasound-electrical stimulation in a band-aid-like way. *Adv Funct Mater.* 2024;34(44):2407411.
30. Xin S, Song W, Mao J, et al. Therapeutic potential of hesperidin in diabetes mellitus-induced erectile dysfunction through Nrf2-mediated ferroptosis and oxidative stress. *Andrology.* 2024. doi:10.1111/andr.13814
31. Fan Q, Chang H, Tian L, et al. Methane saline suppresses ferroptosis via the Nrf2/HO-1 signaling pathways to ameliorate intestinal ischemia-reperfusion injury. *Redox Rep.* 2024;29(1):2373657. doi:10.1080/13510002.2024.2373657
32. Wang M, Wang J, Wang L, et al. Icariside II prevents kidney fibrosis development in chronic kidney disease by promoting fatty acid oxidation. *Phytother Res.* 2024;38(2):839–855. doi:10.1002/ptr.8085
33. Chi A, Yang B, Cao X, et al. ICA II alleviates testicular torsion injury by dampening the oxidative and inflammatory stress. *Front Endocrinol.* 2022;13:871548. doi:10.3389/fendo.2022.871548
34. Wang Z, Mao Y, Zang Y, et al. Transcriptomic analysis reveals the mechanism of isorhamnetin in the treatment of diabetes mellitus erectile dysfunction. *Free Radic Biol Med.* 2024;224:366–381. doi:10.1016/j.freeradbiomed.2024.08.043
35. Zhou B, Chen Y, Yuan H, et al. NOX1/4 Inhibitor GKT-137831 improves erectile function in diabetic rats by ROS reduction and endothelial nitric oxide synthase reconstitution. *J Sexual Med.* 2021;18(12):1970–1983. doi:10.1016/j.jsxm.2021.09.007
36. Qiao H, Zhang Y, Lin W, et al. Decreased expression of pigment epithelium-derived factor within the penile tissues contributes to erectile dysfunction in diabetic rats. *Clin Sci.* 2018;132(20):2175–2188. doi:10.1042/CS20180192
37. Yang X-D, Yang -Y-Y. Ferroptosis as a novel therapeutic target for diabetes and its complications. *Front Endocrinol.* 2022;13:853822. doi:10.3389/fendo.2022.853822
38. Yi M, Cruz Cisneros L, Cho EJ, et al. Nrf2 pathway and oxidative stress as a common target for treatment of diabetes and its comorbidities. *Int J Mol Sci.* 2024;25(2):821. doi:10.3390/ijms25020821
39. Niu C, Jiang D, Guo Y, et al. Spermidine suppresses oxidative stress and ferroptosis by Nrf2/HO-1/GPX4 and Akt/FHC/ACSL4 pathway to alleviate ovarian damage. *Life Sci.* 2023;332:122109. doi:10.1016/j.lfs.2023.122109
40. Liu X-J, Lv Y-F, Cui W-Z, et al. Icaritin inhibits hypoxia/reoxygenation-induced ferroptosis of cardiomyocytes via regulation of the Nrf2/HO-1 signaling pathway. *FEBS Open Bio.* 2021;11(11):2966–2976. doi:10.1002/2211-5463.13276
41. Dang R, Wang M, Li X, et al. Edaravone ameliorates depressive and anxiety-like behaviors via Sirt1/Nrf2/HO-1/Gpx4 pathway. *J Neuroinflammation.* 2022;19(1):41. doi:10.1186/s12974-022-02400-6
42. Zheng Q, Xing J, Li X, et al. PRDM16 suppresses ferroptosis to protect against sepsis-associated acute kidney injury by targeting the NRF2/GPX4 axis. *Redox Biol.* 2024;78:103417. doi:10.1016/j.redox.2024.103417

Drug Design, Development and Therapy

Dovepress
Taylor & Francis Group

Publish your work in this journal

Drug Design, Development and Therapy is an international, peer-reviewed open-access journal that spans the spectrum of drug design and development through to clinical applications. Clinical outcomes, patient safety, and programs for the development and effective, safe, and sustained use of medicines are a feature of the journal, which has also been accepted for indexing on PubMed Central. The manuscript management system is completely online and includes a very quick and fair peer-review system, which is all easy to use. Visit <http://www.dovepress.com/testimonials.php> to read real quotes from published authors.

Submit your manuscript here: <https://www.dovepress.com/drug-design-development-and-therapy-journal>